

Optimal pulse spacing for dynamical decoupling in the presence of a purely-dephasing spin-bath

Ashok Ajoy,^{1,2,3,*} Gonzalo A. Álvarez,^{1,†} and Dieter Suter^{1,‡}

¹*Fakultät Physik, Technische Universität Dortmund, D-44221 Dortmund, Germany.*

²*Birla Institute of Technology and Science - Pilani, Zuarinagar, Goa - 403726, India.*

³*NMR Research Centre, Indian Institute of Science, Bangalore - 560012, India.*

Maintaining quantum coherence is a crucial requirement for quantum computation; hence protecting quantum systems against their irreversible corruption due to environmental noise is an important open problem. Dynamical decoupling (DD) is an effective method for reducing decoherence with a low control overhead. It also plays an important role in quantum metrology, where for instance it is employed in multiparameter estimation. While a sequence of equidistant control pulses (CPMG) has been ubiquitously used for decoupling, Uhrig recently proposed that a non-equidistant pulse sequence (UDD) may enhance DD performance, especially for systems where the spectral density of the environment has a sharp frequency cutoff. On the other hand, equidistant sequences outperform UDD for soft cutoffs. The relative advantage provided by UDD for intermediate regimes is not clear. In this paper, we analyze the relative DD performance in this regime experimentally, using solid-state nuclear magnetic resonance. Our system-qubits are ¹³C nuclear spins and the environment consists of a ¹H nuclear spin-bath whose spectral density is close to a normal (Gaussian) distribution. We find that in the presence of such a bath, the CPMG sequence outperforms the UDD sequence. An analogy between dynamical decoupling and interference effects in optics provides an intuitive explanation as to why the CPMG sequence performs superior to any non-equidistant DD sequence in the presence of this kind of environmental noise.

PACS numbers: 03.65.Yz, 03.67.Pp, 76.60.-k, 76.60.Lz

I. INTRODUCTION

Quantum information processing (QIP) relies on storing and manipulating information in quantum mechanical states associated with accessible subunits called qubits [1]. For reliable QIP, the information encoded in the quantum register (the collection of qubits) must be retained for arbitrarily long time [2]. However, in any physically realizable QIP architecture, the qubits cannot be completely isolated, but are weakly coupled to a large number of degrees of freedom of their environment (bath). This causes the corruption of the quantum state associated with the qubit, a process known as decoherence [3]. This process limits the time scale over which quantum information can be retained [3] and the distance over which it can be transmitted [4–7].

Combating this decoherence process to extend the life time of quantum states or processes and the distance bounds to transmit them is a necessary step in building a quantum computer [8]. One of the simplest and most effective techniques suggested for this purpose is Dynamical Decoupling (DD) [9, 10]. It also has several applications in quantum metrology, for example in the magnetometry using single spins [11–13] and multiparameter estimation [14]. DD consists of the application of π -pulses to the qubits, which revert the decay due to the system-

environment interaction. The simplest implementation of this method is the Hahn echo experiment [15]. It is employed in the case when the system-environment (SE) interaction is a pure dephasing process – i.e. there is no net exchange of energy between the system and the bath.

However, it is immediately obvious that any component of the interaction with the bath that varies on a time scale shorter than τ , the delay between the pulses, cannot be refocused [16, 17]. Hence the effectiveness of the Hahn echo and its generalization as a train of equidistant pulses – the CP [16] and CPMG [17] sequences – depend crucially on keeping the delays τ between the pulses sufficiently short. However, this delay is always limited by hardware or the maximum power deposition in the sample. Moreover, rapid DD pulsing interferes with the controls that are necessary for computation [18, 19]. For example, if one wants to choreograph the dynamics of the spins in a particular manner while still requiring that coherence survives for long, the requisite controls have to be applied in parallel with the DD pulses. Although the recent proposal of Dynamically Corrected Gates (DCGs) [20–23] seeks to address this problem, when τ is very short there is an enormous demand on the hardware.

Hence there is a strong motivation for finding a DD protocol that, for a given number of pulses, provides the best performance. For the case of a purely dephasing SE interaction, a possible approach to this problem consists in visualizing the DD pulses as generating a filter for the SE interaction (environmental modes) [24, 25]. For example, the CPMG sequence acts as a band-stop or high-pass filter (with bandwidth $\omega = 2\pi/\tau$) since any interaction component that varies slower than τ is refocused and fil-

*Electronic address: ashok.ajoy@gmail.com

†Electronic address: galvarez@e3.physik.uni-dortmund.de

‡Electronic address: Dieter.Suter@tu-dortmund.de

tered out. The resulting decay rate of the quantum state is determined by the overlap of the spectral density of the bath with the filter generated by the pulse sequence [24, 25]. If one knows the exact form of this function, it may be possible to design a suitable filter, and hence a DD sequence, that leads to the slowest decay [25–31]. This was the motivation behind the DD sequence suggested by Uhrig [26]. It provides the non-equidistant distribution of pulses that causes the flattest band-stop filter around $\omega = 0$ [24, 32], and is considered the best sequence for combating low frequency noise. Experimental work [28, 33–35] showed that indeed UDD outperforms CPMG for certain types of noise with a sharp high-frequency cut off.

However, when the spectral density of the bath has a long tail (soft cutoff), the CPMG sequence has been predicted [24, 36] and found [28, 33] to outperform the UDD sequence. In an intermediate regime, for example a spin-bath where the spectral density is Gaussian [37], it was shown recently that CPMG outperforms the UDD sequence [38–41]. However, a rigorous comparison of both these sequences in such regimes is a matter of current research [25, 42–45]. Of particular interest is determining the conditions (for example, the maximum allowable τ) under which the UDD continues to provide an advantage over CPMG.

This was tackled in a purely dephasing bosonic bath by Hodgson *et al.* [43]. They predicted that DD protocols with non-equidistant pulses like UDD lose their advantages when lower bounds exist for the pulse separation τ . Uhrig and Lidar [46] presented analytical performance bounds for UDD. They considered instantaneous perfect pulses and bounded environment and generic system-environment Hamiltonians. They showed that for a fixed total duration, the survival probability can be increased by increasing the number of pulses by incrementing the DD order. However, if a minimum delay between pulses is imposed, because the sequence time scales with the number of pulses (DD order), they predict that longer cycles (higher orders) are not always advantageous. These predictions are based on perturbative treatments of the SE interaction. Accordingly, they apply to the fast control regime where the cycle time is sufficiently short for the perturbative treatment. Because these approaches cannot lead to a lower bound on the attainable DD error in the presence of timing constraints, recently Khodjasteh *et al.* [45] obtained bounds for the UDD performance as a function of its order by using an alternative method for bosonic baths.

In light of this, it is important to provide a fair and practically relevant comparison between these different DD approaches. Here, we use the benchmarking methodology of our previous work [38]: which DD sequence maximizes the survival time of the quantum coherence for a given average spacing between the pulses? In the earlier paper, we concentrated on a comparison between different sequences with equidistant pulses; here, we analyze the effect of a variable pulse spacing, using the same

approach. The spectral density of our bath is roughly Gaussian, which may be considered to be intermediate between a sharp cutoff and a long tail.

Several recent experimental results [38–41] indicate that CPMG performs better than UDD when the qubit is coupled to a spin-bath. The superior CPMG performance has been attributed to the fact that it compensates pulse errors along the direction of the rotation axis [40, 41], while such compensation is reduced in UDD [28, 33]. Also it was attributed to a possible soft-cut off of their model system [39–41]. Our experiments and simulations indicate that even in the case of ideal pulses, the CPMG outperforms UDD. In fact, we conjecture that for a purely dephasing SE interaction, when the spectral density is a Gaussian distribution and a rapidly fluctuating environment, the CPMG sequence would maintain the state of the qubit system for the longest period. Our reasoning is based on determining how the DD pulse sequence alters the time-averaged SE interaction that the system “sees”, for each frequency component of this interaction [24]. Drawing an analogy with optics, each pulse of the Uhrig sequence modifies the SE interaction such that the interactions in different windows “interfere” destructively with each other. This destructive interference is perfect for slow interactions. While the UDD protocol provides the *flattest* stop-band at $\omega = 0$ [24], the CPMG protocol provides the *widest*. When a DD sequence is applied repetitively (say M times), it becomes analogous to passing the different frequency components of the SE interaction through a diffraction grating. Overall, the optical analogy presented in this paper provides an intuitive way to understand how the shape of the spectral density function affects DD performance.

This paper is organized as follows. Sec. II describes the physical system that we use in our experiments. In Sec. III we review the key ideas of dynamical decoupling. Sec. IV provides the pulse sequence protocols of UDD [26, 32] and CPMG [16, 17]. Sec. V contains the results of our experiments. Sec. VI describes a semi-classical model that explains the experimental results, and suggests that the CPMG sequence is the best DD sequence for combating a purely-dephasing SE interaction in a spin-bath. Within this section we draw an optical analogy to DD sequences.

II. THE SYSTEM

For our experimental evaluation of the relative performance of DD sequences, we use the simplest possible system consisting of a single qubit and a purely dephasing environment consisting of a spin-bath. For the system qubit, we use ^{13}C nuclear spins ($S = 1/2$), and for the environment ^1H nuclear spins ($I = 1/2$) that act as the spin-bath. We use polycrystalline adamantane where the natural abundance of the ^{13}C nuclei is about 1%, and to a good approximation each ^{13}C nuclear spin is surrounded by about 100 ^1H nuclear spins. The ^{13}C - ^{13}C interaction

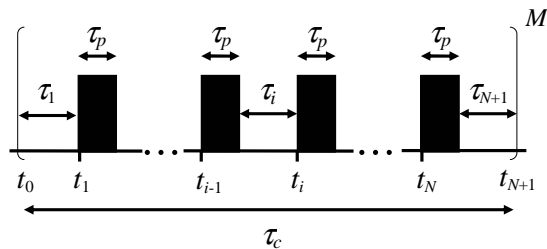


Figure 1: Schematic representation of dynamical decoupling. The solid boxes represents the control pulses.

is completely negligible compared to the ^{13}C - ^1H and ^1H - ^1H interactions. The spin-spin interaction is dominated by the dipolar interaction [37].

We shall refer to the spin operator of the system qubit (^{13}C) as \hat{S} , and to the j^{th} bath spin (^1H) as \hat{I}^j . The Zeeman frequencies of the system- and bath spins are ω_S and ω_I , respectively. The dipolar coupling constants for the system-bath interaction are b_{Sj} , and for the intra-bath interaction d_{ij} .

It is convenient to describe the dynamics of the system in a rotating frame of reference [37], where the system rotates at the (angular) frequency ω_S around the z -axis and the environment at ω_I . The total (free evolution) Hamiltonian is then

$$\hat{\mathcal{H}}_f = \hat{\mathcal{H}}_S + \hat{\mathcal{H}}_{SE} + \hat{\mathcal{H}}_E, \quad (1)$$

where $\hat{\mathcal{H}}_S$ is the system Hamiltonian, $\hat{\mathcal{H}}_E$ the environment Hamiltonian and $\hat{\mathcal{H}}_{SE}$ the system-environment interaction Hamiltonian:

$$\hat{\mathcal{H}}_S = \hat{0}, \quad (2)$$

$$\hat{\mathcal{H}}_{SE} = \hat{S}_z \sum_j b_{Sj} \hat{I}_z^j, \quad (3)$$

$$\hat{\mathcal{H}}_E = \sum_{i < j} d_{ij} \left[2\hat{I}_z^i \hat{I}_z^j - (\hat{I}_x^i \hat{I}_x^j + \hat{I}_y^i \hat{I}_y^j) \right]. \quad (4)$$

This type of system is encountered in a wide range of solid-state spin systems, as for example electron spins in diamonds [39, 41, 47], electron spins in quantum dots [40, 48, 49] and donors in silicon [50, 51], which appear to be promising candidates for future QIP implementations. In particular, we consider the case where the interaction with the bath is weak or comparable with the intra-bath interaction.

III. DYNAMICAL DECOUPLING

Dynamical decoupling aims to reduce the interaction of the system with the environment by applying sequences of short, strong pulses that invert the system qubits [9, 10]. We write $\hat{\mathcal{H}}_{C(S)}(t)$ for the corresponding control Hamiltonians. It is assumed that the environment cannot be directly controlled.

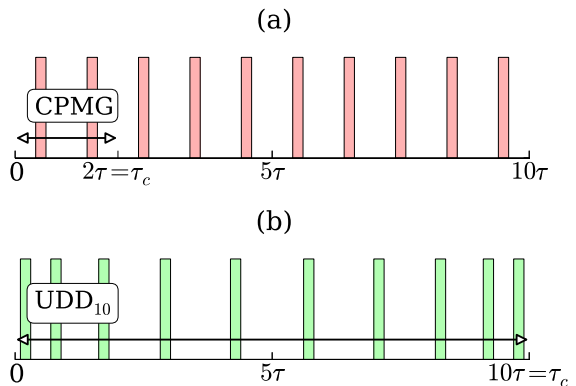


Figure 2: (Color online) Distribution of pulses for (a) CPMG and (b) UDD_{10} sequences. Here τ is the average distance between pulses. The arrows denote the length of a single cycle of period τ_c . Note that a CPMG cycle consists of 2 pulses while an N^{th} order UDD cycle has N pulses.

DD sequences usually consist of cycles of pulses. Figure 1 shows an example of such a cycle. In the rotating frame, the operator that describes the evolution of the total system from 0 to τ_c , the duration of the cycle, is

$$\hat{U}(\tau_c) = \hat{U}_f(\tau_{N+1}) \prod_{i=1}^N \hat{U}_C^i(\tau_p) \hat{U}_f(\tau_i), \quad (5)$$

where the free evolution operator is

$$\hat{U}_f(t) = \exp\{-i\hat{\mathcal{H}}_f t\} \quad (6)$$

and the control evolution operators are

$$\hat{U}_C^i(\tau_p) = T \exp\left\{-i \int_0^{\tau_p} dt' \left(\hat{\mathcal{H}}_f + \hat{\mathcal{H}}_{C(S)}^i(t')\right)\right\}, \quad (7)$$

where T is the Dyson time-ordering operator [52, 53] and τ_p the pulse duration. Let t_i represent the time at which the i^{th} control operation starts. Then, the delay times between the control Hamiltonians are $\tau_i = t_i - (t_{i-1} + \tau_p)$ for $i = 2, \dots, n+1$ and $\tau_1 = t_1 - t_0$, where $t_0 = 0$ and $t_{N+1} = \tau_c$. If the basic cycle is iterated M times (see Fig. 1), the total evolution operator becomes

$$\hat{U}(t = M\tau_c) = \left[\hat{U}(\tau_c)\right]^M. \quad (8)$$

The propagator (5) for a single cycle of duration τ_c can be written in terms of an effective Hamiltonian:

$$\hat{U}(\tau_c) = e^{-i\hat{\mathcal{H}}_{eff}\tau_c}. \quad (9)$$

Using average Hamiltonian theory [54] $\hat{\mathcal{H}}_{eff}$ can be expressed as a series expansion, using, e.g., the Magnus expansion [55],

$$\hat{\mathcal{H}}_{eff} = \hat{\mathcal{H}}^{(0)} + \hat{\mathcal{H}}^{(1)} + \hat{\mathcal{H}}^{(2)} + \dots = \sum_{m=0}^{\infty} \hat{\mathcal{H}}^{(m)}. \quad (10)$$

The lowest order term $\widehat{\mathcal{H}}^{(0)}$ is the average over the period τ_c ,

$$\widehat{\mathcal{H}}^{(0)} = \frac{1}{\tau_c} \int_0^{\tau_c} \widehat{\mathcal{H}}(t) dt. \quad (11)$$

A DD sequence with ideal pulses makes $\widehat{\mathcal{H}}^{(0)} = \widehat{\mathcal{H}}_E$, i.e., the interaction Hamiltonian vanishes to zeroth order. In addition, the DD sequences are designed such that the higher order terms have reduced norm or vanish [10, 26, 56].

As we discussed in the previous section, the ^{13}C - ^{13}C dipolar interaction is negligible compared with the ^{13}C - ^1H interaction. However, when DD is active and removes the ^{13}C - ^1H interaction, the ^{13}C - ^{13}C couplings become the dominant interaction for causing decoherence. This holds strictly for ideal pulses, which do not affect the ^{13}C - ^{13}C interaction. Under these conditions, the decay rate is limited by the ^{13}C - ^{13}C couplings. However, if pulses have finite duration, they can further extend the lifetime of the component of the magnetization aligned with the effective field [57–63].

IV. PULSE SEQUENCES

A. Carr-Purcell (CP) and Carr-Purcell-Meiboom-Gill (CPMG)

The Carr-Purcell (CP) sequence [16] was first introduced as a means to suppress inhomogeneity of the B_0 field ΔB_0^j seen at the j^{th} nuclear site when the molecules containing the spins are undergoing diffusion. The resulting time-dependent system-environment interaction interferes with the refocusing process of a Hahn echo [15] if the time dependence happens on a time scale comparable to or faster than the refocusing time.

In our solid-state spin system, the time dependence of the environment arises from fluctuating dipolar fields due to the neighboring spins of the bath [54]. This generates a time-dependent inhomogeneity. By suppressing it, the CP sequence acts as a method of dynamical decoupling since, in effect, it suppresses the SE interaction [9].

The CP sequence consists of a train of refocusing pulses generating spin-echoes. If the refocusing pulses are ideal, i.e., they cause a complete π rotation of the nuclear spins in an infinitesimal time, and the spin-bath is static ($[\widehat{\mathcal{H}}_E, \widehat{\mathcal{H}}_{SE}] = \hat{0}$), then all terms $\widehat{\mathcal{H}}^{(m)}$ of the Magnus expansion vanish, and the inhomogeneity is completely suppressed. However, this does not happen when the spin-bath is not static or the pulses have finite duration or contain errors. For ideal pulses but a fluctuating environment only the average system environment Hamiltonian $\widehat{\mathcal{H}}_{SE}^{(0)}$, the zeroth order of the Magnus expansion, is suppressed [38].

If flip-angle errors are also considered, the system-environment coupling no longer vanishes, even in lowest order, $\widehat{\mathcal{H}}_{SE}^{(0)} \neq \hat{0}$, and the resulting propagator increases

with the flip-angle error. Considering this, Meiboom and Gill suggested a modification to the CP sequence [17], now called the CPMG sequence, where the rotation axis of the pulses is the same as the orientation of the initial state of the spins. In this case, flip-angle errors have no effect in zeroth order. Fig. 2a shows a CPMG sequence. Note that the CPMG cycle requires only 2 pulses; hence a sequence of 10 pulses covers 5 cycles. In the figure, τ is the average distance between pulses, while τ_c denotes the length of a single cycle.

B. Uhrig dynamical decoupling (UDD)

In the CPMG sequence, the separation between adjacent pulses is constant throughout the sequence. In a seminal paper [26, 32], Uhrig relaxed this condition, searching for the optimal combination of delays that would minimize the effect of a purely dephasing system-environment coupling. He showed that the optimal distribution for reducing low-frequency noise corresponds to a sinusoidal modulation of the pulse delays. More specifically, one cycle of an N^{th} order UDD sequence consists of N pulses applied at times

$$t_i = \tau_c \sin^2 \left[\frac{\pi i}{2(N+1)} \right], \quad (12)$$

where $t_{N+1} = \tau_c$ is the cycle time and $t_0 = 0$ the starting time. Fig. 2b shows the UDD sequence for $N = 10$. The CPMG sequence is the simplest UDD sequence with order $N = 2$. The UDD sequence was shown to be universal for any purely dephasing Hamiltonian [64].

V. EXPERIMENTS

A. Measurement scheme

The general procedure used in our experiments is illustrated in Fig. 3. Cross-polarization from the abundant proton spins to the ^{13}C spins is used at the initial preparation stage to increase the ^{13}C polarization [65]. After this transfer, we store the enhanced ^{13}C polarization along the z axis and wait for a time longer than the dephasing time to erase any correlation that could arise during the cross-polarization process. The magnetization is then rotated to an initial state, represented by the density operator $\hat{\rho}_0 = \hat{S}_{\{x,y\}}$, in the xy -plane that is transverse to the strong static field. We use two distinct initial states considering the relative phases of the polarization of $\hat{\rho}_0$ and the pulses to be used for DD [28, 38]—the “longitudinal” state in Fig. 4(a) where the pulses are applied in the direction of the $\hat{\rho}_0$ polarization, and the “transverse” state in Fig. 4(b) where they are applied perpendicular to the $\hat{\rho}_0$ polarization. This translates, in Fig. 3, to applying the DD π pulses with an X phase where a $\pi/2$ pulse is applied before of the DD sequence

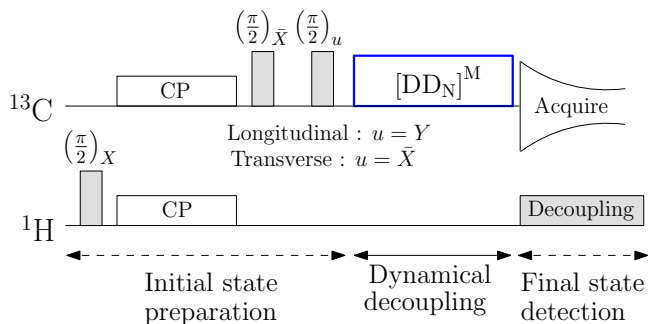


Figure 3: (Color online) The experimental scheme: the initial state preparation uses cross-polarization (CP) to enhance the polarization of the ^{13}C nuclear spins. The actual dynamical decoupling consists of M cycles of the N -order DD sequence. The DD pulses are applied along the X axis, while the initial states are created using a $(\frac{\pi}{2})$ pulse with Y ($-X$) phase for the longitudinal (transverse) initial conditions.

with a Y phase for the longitudinal initial condition, and with a $-X$ phase for the transverse condition. M cycles of the N -pulse DD sequence are applied; the duration for the DD π pulses was $10.4 \mu\text{s}$. The errors of the pulse delays (compared to the theoretical values) are 2.5 ns on average, limited by the timing resolution of our pulse generator. The error of the pulse durations (jitter) is $< 0.1 \text{ ns}$. Therefore timing errors are negligible compared to amplitude errors, which are of the order of 10% . In general for the range of delays between pulses used in our experiments, we did not observe substantial differences between considering the delays from the pulse edges or centers. This was also corroborated by numerical simulations. After each DD cycle, we measured the remaining spin polarization by recording the NMR signal [38]. During the signal acquisition, we applied continuous wave decoupling to prolong the FID and thereby increase the detection sensitivity.

The decay of the signal amplitude as a function of the DD evolution time $t = M\tau_c$ represents the survival probability of the state $\hat{\rho}_0$:

$$s(t) = \frac{\text{Tr}\{\hat{\rho}_0\hat{\rho}(t)\}}{\text{Tr}\{\hat{\rho}_0\hat{\rho}_0\}},$$

where $\hat{\rho}(t) = \hat{U}(t)\hat{\rho}_0\hat{U}^\dagger(t)$ is the density operator of the spin-system at time t . In the case of free evolution (no DD), this corresponds to the free induction decay signal represented in Fig. 5. The solid blue lines in panels (a) and (b) represent the FID signal of the ^1H and ^{13}C spins, respectively, which correspond to the observables \hat{I}_x and \hat{S}_x .

B. Single parameter three pulse family

We first consider the simplest sequence that contains unequal spacings between the pulses. Fig. 6 (a) and (b) show the time evolution of the ^{13}C magnetization from a

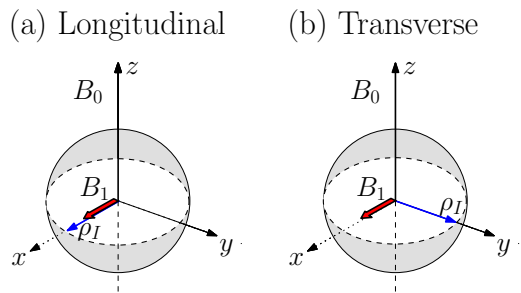


Figure 4: (Color online) Different initial states of the spin system: The blue (thin, long) arrows indicate the orientation of the initial ^{13}C -spin polarization, and the red (thick, short) arrows show the direction in which the pulses are applied.

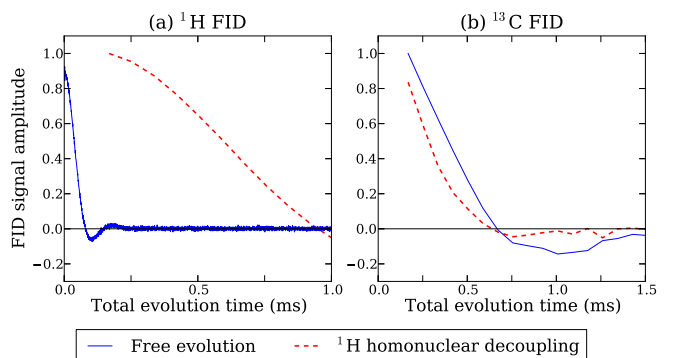


Figure 5: (Color online) Experimental FID of (a) ^1H and (b) ^{13}C spins without (blue solid line) and with (red dashed line) BLEW-12 ^1H homonuclear decoupling. The correlation time of the bath (^1H) increases by an order of magnitude if the BLEW-12 sequence is applied. The qubit system (the ^{13}C nuclei) remains almost unaffected by the BLEW-12 sequence.

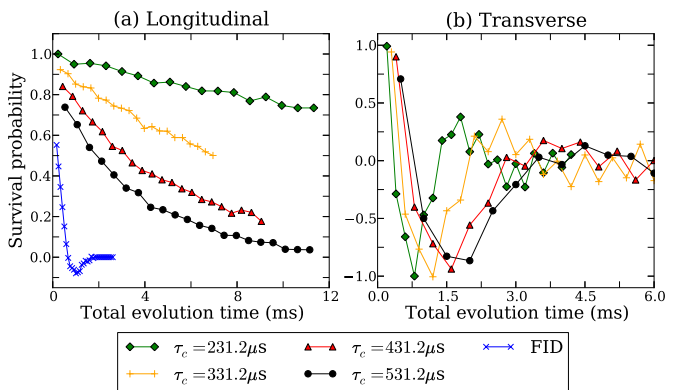


Figure 6: (Color online) Time evolution of the ^{13}C magnetization of the initial state (proportional to its survival probability), for the (a) longitudinal and (b) transverse initial conditions subjected to UDD₃. The value of -1 in the latter corresponds to the state that is antiparallel to the initial state.

longitudinal initial state $\hat{\rho}_0 = \hat{S}_x$ and a transverse initial state $\hat{\rho}_0 = \hat{S}_y$ for different cycle times. They show that when the longitudinal case is compared to the FID, dynamical decoupling allows for a longer survival of coherence, and this improves for shorter cycle times [38]. The signal decay is an order of magnitude faster for the transverse initial condition in Fig. 6(b), than the longitudinal condition 6(a) [38]. As we demonstrated in Ref. [38], in this case the decay is due mostly to pulse imperfections (flip-angle errors), which lead to a loss of polarization. In the longitudinal case, the effect of these pulse errors is partly compensated over the sequence, but in the transverse case, they accumulate. This accounts for the large difference between the two cases already demonstrated in previous works [33, 38]. In particular in our experimental setup, the flip-angle error was estimated to be around 10% [38].

Uhrig introduced the idea that it might be advantageous to omit the condition that all pulse separations should be identical and derived a simple formula that determines the optimal spacing of N pulses. We examine this scheme first in the simplest possible case, corresponding to a cycle of 3 pulses. In order to determine the optimal pulse spacing experimentally, we parametrize the pulse spacings of the symmetric three-pulse sequence with a parameter x , as shown in Fig. 7(a). x is defined as the deviation (as a fraction of the cycle time) of the pulse separation from those of the UDD₃ sequence, which are $\tau_1 = \tau_c \sin^2(\pi/8)$ and $\tau_2 = \tau_c/2 - \tau_1$. This parametrization captures all possible mirror symmetric three-pulse sequences. When $x = 0$, the sequence is UDD₃, and when $x \simeq 0,0203$, the sequence is CPMG. For this family of DD sequences, we experimentally determined the decay rate as a function of x by fitting a pure exponential function.

Figure 8 shows the experimentally obtained decay rates for the longitudinal initial condition, as a function of the parameter x . We determined the value of x that generates the slowest decay rate by fitting the experimental data points with a quadratic function (not shown in the figure) and determining the position of the minimum. These minima are the red circles in Fig. 9. The sequence that generates the slowest decay is obtained for $x_{min} \approx 0.021 \pm 0.002$, for all cycle times used in the experiment. This is astonishingly close to the value $x_{CPMG} = 0.0203$ that corresponds to the equally spaced sequence.

In addition to the experimental data points, Fig. 8 also shows solid lines. They represent the results of numerical simulations of the decay rates for the same parameters as the experiments. In the simulations, we assumed that the pulses were ideal. Following Ref. [24, 32] this involves modeling the pulse sequence as a one-dimensional filter $f(\tau, \tau_c)$, as shown in 7(b). A detailed description of this model and the simulations is presented in Sec. VI. Since this model does not take into account pulse errors, it cannot be applied to the transverse initial condition, where these errors play a predominant role [38].

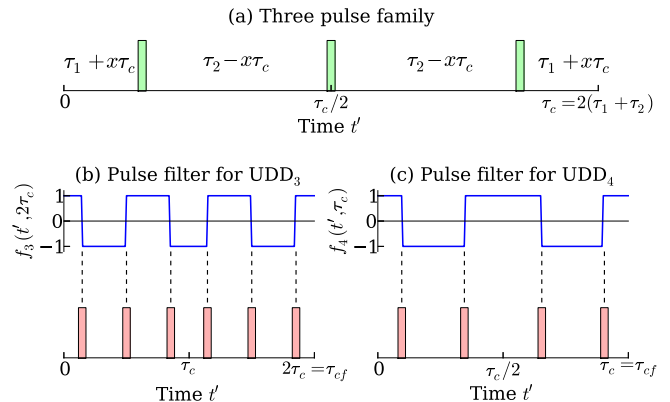


Figure 7: (Color online) (a) Single parameter sequence family containing all mirror symmetric three-pulse sequences. They are described by the parameter x , where τ_1 and τ_2 are the exact UDD₃ delays. (b) Time domain filter function $f_3(\tau', 2\tau_c)$ for two cycles of the UDD₃ sequence. (c) Time domain filter function $f_4(\tau', \tau_c)$ for one cycle of the UDD₄ sequence. In the filter representation we assume perfect pulses in the center of the finite-width pulses. The dashed lines indicate that the time domain filter toggles between ± 1 at the position of the pulses.

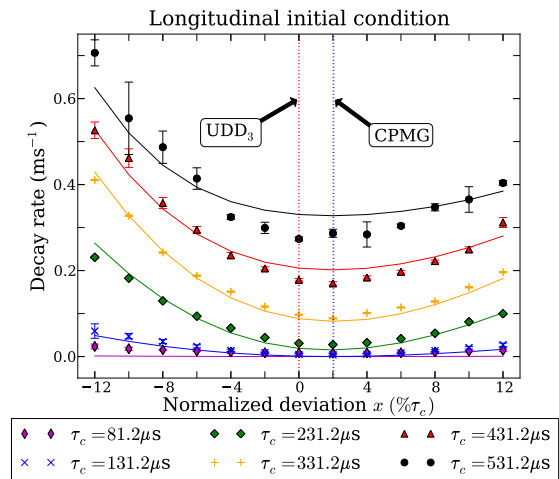


Figure 8: (Color online) Experimental (symbols) and simulated (lines) decay rates of the magnetization as a function of the deviation x for different cycle times for the longitudinal initial condition. The UDD₃ sequence corresponds to $x_{UDD} = 0$, while the CPMG sequence corresponds to $x_{CPMG} \approx 0.0203$. Note that the quadratic fitting curves used to determine to position of the minimum of each curve are not shown.

For the transverse initial condition, the rates are about an order of magnitude larger than for the longitudinal initial condition, and they increase for short cycle times [38]. They are essentially independent of the parameter x because they are dominated by pulse errors. We therefore consider only longitudinal states in the following.

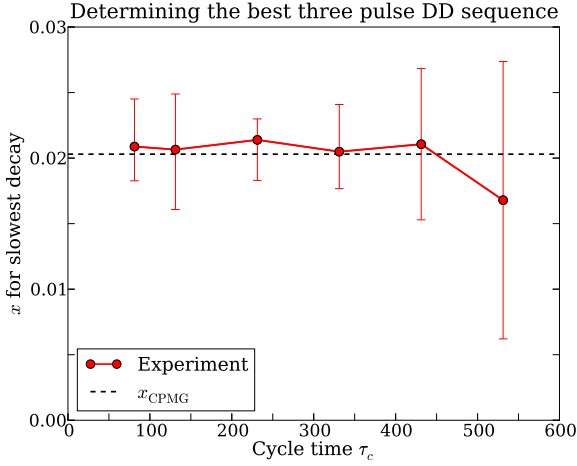


Figure 9: (Color online) In order to determine the best longitudinal three-pulse DD sequence, the decay curves in Fig. 8 were fitted to a quadratic function in the region of the minimum. The positions of the minima of these quadratic fits are represented by the red circles in this figure. The black dotted line corresponds to $x_{\text{CPMG}} \approx 0.0203$.

C. Variation of UDD order

The performance of a dynamical decoupling sequence increases with the average power of the external control field used for DD [9]. This means that given a fixed time window t , the DD efficiency improves with the number of refocusing pulses. Since the pulses are of finite length, the maximum number of pulses that can be employed during t is bounded [19, 38, 42, 43, 45, 46].

The scheme depicted in Fig. 10(a) describes a situation in which the cycle time τ_c is fixed, while the UDD order is increased from top to bottom. Given the fixed window $t = \tau_c$, the power used for DD during t increases from top to bottom. The corresponding survival probability is shown in Fig. 10(c) for different UDD orders (from UDD₂ to UDD₁₄) and with $\tau_c = 600\mu\text{s}$ (not including the pulse lengths). Clearly, if the cycle time is fixed, higher order UDD sequences maintain the qubit coherence for longer times. However, this improved performance is obtained at the price of an increase in the average power applied to the system. For many applications, this is not possible, and a more meaningful comparison is obtained by keeping the average power level fixed. Fig. 10(b), shows the corresponding pulse sequences and Fig. 10(d) the resulting decays. For these experiments, the cycle time was scaled with the UDD order N as $\tau_c = N 110.4\mu\text{s}$. Under these conditions, the variation of the decay rate with the UDD order is relatively weak and higher orders perform slightly worse than UDD₂(CPMG).

We quantified the decay rates for UDD orders 2 to 30 for $\tau_c = N 110.4\mu\text{s}$. The results are shown in the right panel of Fig. 11. The left panel schematizes how the DD power is kept constant across orders – the cycle time is

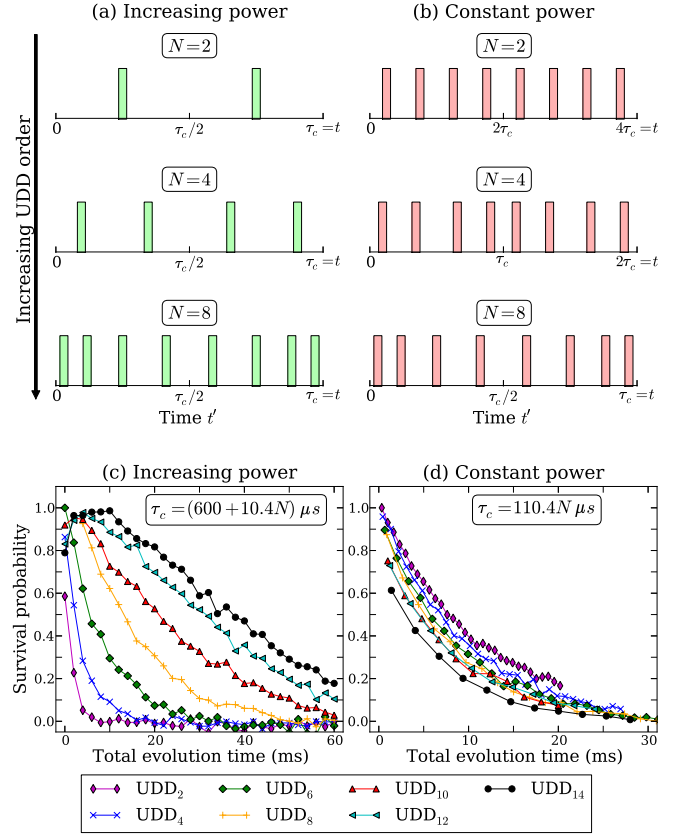


Figure 10: (Color online) Top panels: Pulse sequence scheme keeping fixed the time window t as the UDD order N is increased. To keep the DD power constant across UDD orders, the cycle time is scaled with N (b). Bottom panels: Experimental ^{13}C signal decay for different UDD orders for (c) a fixed cycle time $\tau_c = 600\mu\text{s}$, (d) a scaled cycle time $\tau_c = 110.4N\mu\text{s}$.

scaled with the UDD order. Clearly, for a large span of UDD orders, the CPMG sequence performs better than the UDD. The results mean two things: first, that in the regime of our experiment, higher UDD orders provide no advantage over lower UDD orders; and second, that in consequence the UDD protocol itself performs worse than the CPMG sequence with the same number of pulses. Although these experiments were carried out with the average delay between pulses of $110.4\mu\text{s}$, the same qualitative behavior is also observed for different times between pulses. However, the difference between the decay rates of CPMG and UDD can be reduced by shortening the cycle time as we show below.

D. Variation of cycle time

In the limit of infinitesimally short cycle time and infinitely strong pulses – the *bang-bang* regime [9]– one can maintain quantum coherence for arbitrarily long times. However, in any real experiment, the peak power as well

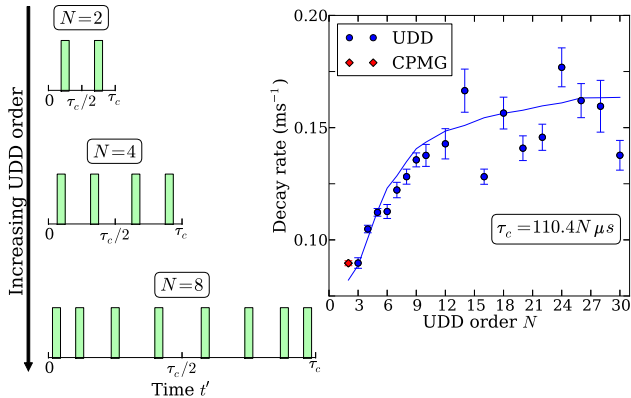


Figure 11: (Color online) Left panel: Pulse scheme manifesting the cycle time scaling with the UDD order N . Right panel: Experimental (symbols) and simulated (line) decay rates of the ¹³C magnetization for different UDD orders (blue circles) compared with decay rates achieved with the CPMG sequence (red rhombus). The same number of pulses during a time window t are applied by scaling the cycle time as $\tau_c = 110.4N \mu s$.

as the average power applied to the system are limited and should be minimized. Accordingly, the duration of the pulses and the cycle time cannot be reduced below some minimal values [19, 38, 42, 43]. In this section, we examine the DD performance of a given sequence as a function of the cycle time. The left panel of Fig. 12 schematically describes the variation of the cycle time for a fixed UDD order N , in this case for $N = 5$. In the right panel of Fig. 12, the points are experimentally obtained decay rates while the lines are simulation results using the filter model for ideal pulses detailed in Sec. VI. For long cycle times, the performance of equidistant pulses (CPMG) is better than UDD however as τ_c is reduced its performance improves considerably, although the UDD decay rates are indistinguishable from the CPMG in this regime. Similar results were obtained for similar experiments with different UDD orders. Fig. 12 shows that in the regime of our experimental setup, UDD does not perform better than the CPMG for any τ_c .

E. Reducing the fluctuation rate

The decay rate of the survival probability under dynamical decoupling depends on the ratio of the cycle time τ_c to the correlation time of the bath τ_B [38, 66]. The UDD sequence was designed to provide optimal decoupling performance for baths with long correlation times. In our system, the bath correlation time depends on the strength of the dipolar couplings d_{ij} between the ¹H nuclear spins of the bath [37]. One can effectively rescale d_{ij} , and hence the correlation time of the bath, by applying decoupling sequences to the bath spins [54]. This allows us to access regimes where the cycle time τ_c is sig-

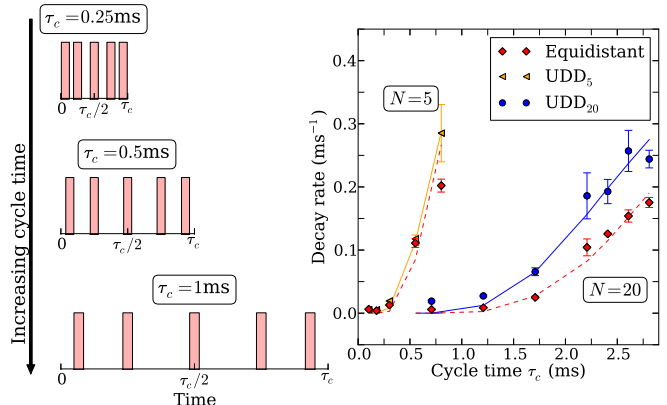


Figure 12: (Color online) Left panel: Pulse sequence scheme showing the variation of its cycle time for a fixed UDD order $N = 5$. Right panel: Experimental (points) and simulated (lines) decay rates of the ¹³C magnetization for UDD₅ and UDD₂₀ and its comparison with equidistant pulse (CPMG) sequence having the same number of pulses for the different UDD cycle times.

nificantly shorter than the correlation time of the bath.. For this we employ the well-known homonuclear decoupling sequence BLEW-12 [67]. As shown by the dashed lines of Fig. 5, application of this pulse sequence increases the bath-correlation time by about one order of magnitude: it was around $\tau_B \approx 100 \mu s$ without BLEW-12 and $\tau_B \approx 1000 \mu s$ with BLEW-12 for a cycle time $\tau_{cB} = 84 \mu s$. To determine the effects on the qubit system, we measured its free induction decay (FID). We found that it remains almost unaffected by the ¹H homonuclear decoupling (Fig. 5b). The scaling due to the BLEW sequence [67], 0.475, appears to be indistinguishable from the effect of self-decoupling, which reduces the ¹³C linewidth in the absence of ¹H-homonuclear decoupling [68]. The experimental scheme of Fig. 2 was used again, the only change being that the homonuclear decoupling sequence is applied to the bath in parallel with the application of the DD sequence to the system.

Figure 13 shows the pulse sequence used during the DD period (left panel). For different UDD orders, the signal decays were measured with and without the BLEW-12 sequence (dashed box in the left panel) on the ¹H channel. The experimental results in the right panel of Fig. 13 show that the increase of the bath correlation time by roughly one order of magnitude leads to significant improvements in the performance of all DD sequences. The performance of UDD₃ and CPMG is indistinguishable, while that of UDD₆ is lower.

Similar results are obtained for longer and shorter cycle times. This is evidenced in Fig. 14(b), which shows the survival probability after a *single* cycle of the UDD and equidistant pulse (CPMG) sequences for different cy-

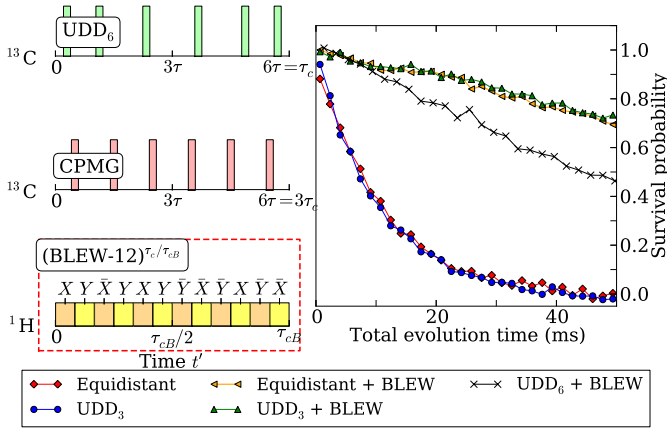


Figure 13: (Color online) Left panel: DD pulse sequence scheme for UDD_6 and CPMG applied in conjunction with the BLEW-12 sequence on the ^1H spin-bath. The cycle time of the DD sequences is 6τ , while for the BLEW-12 sequence the cycle time is τ_{cB} , where $6\tau/\tau_{cB}$ is an integer. Right panel: ^{13}C signal decay for the DD sequences described in the legend.

cle times and DD orders. The pulse sequence for this experiment is shown in Fig. 14(a) for two cycle times $\tau_c = 336\mu\text{s}$ and $\tau_c = 672\mu\text{s}$ of the UDD_{12} sequence. The results show that for large UDD orders like $N = 12$, the CPMG sequence performs better, even when the fluctuations of the environment are slow. For $N = 3$ the performance of both sequences is comparable within experimental errors.

VI. PHYSICAL INTERPRETATION OF THE EXPERIMENTAL RESULTS

A. Semiclassical approximation

In this section, we present a semiclassical model to explain and interpret the experimental results of section V. Since the system is well in the high-temperature limit, it is possible to use a semiclassical description instead of the fully quantum mechanical treatment [37]. Most of the mathematical description of this subsection was developed within the DD context on different systems [24, 32] and they can be obtained from standard semiclassical treatments [37]. Here we connect and reinterpret them to describe our spin system. Starting from the quantum mechanical description of section II, the effect of the environment-Hamiltonian \hat{H}_E on the evolution of the system may be discussed in an interaction representation with respect to the evolution of the isolated environment:

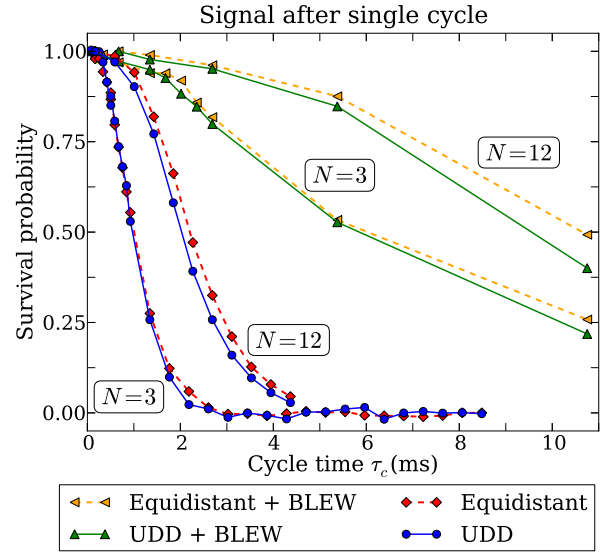
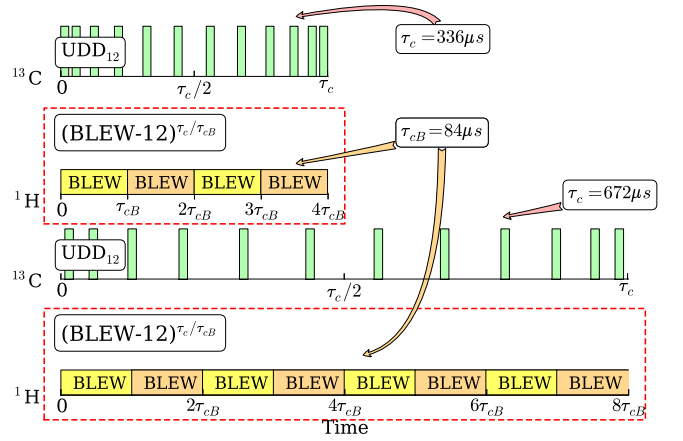


Figure 14: (Color online) (a) UDD_{12} sequence applied with homonuclear decoupling of the ^1H spins. Sequences for two different cycle times $\tau_c = 336\mu\text{s} = 4\tau_{cB}$ and $\tau_c = 672\mu\text{s} = 8\tau_{cB}$, where $\tau_{cB} = 84\mu\text{s}$ is the cycle time of the BLEW-12 homonuclear decoupling sequence. (b) Experimental survival probability (fidelity) of the initial state $\hat{\rho}_I = \hat{S}_x$ for a single cycle with N pulses and varying the cycle time τ_c with and without homonuclear decoupling of the spin-bath.

the system-environment Hamiltonian then becomes

$$\begin{aligned} \hat{H}_{SE}^{(E)}(t) &= e^{-i\hat{H}_E t} \hat{H}_{SE} e^{i\hat{H}_E t} \\ &= \hat{S}_z e^{-i\hat{H}_E t} \left(\sum_j b_{Sj} \hat{I}_z^j \right) e^{i\hat{H}_E t} \end{aligned} \quad (13)$$

$$= b_{SE} \hat{S}_z e^{-i\hat{H}_E t} \hat{E}_z e^{i\hat{H}_E t}, \quad (14)$$

where $\hat{E}_z = \left[\sum_j \frac{b_{Sj}}{b_{SE}} \hat{I}_z^j \right]$ represents an effective spin bath operator and $b_{SE} = \sqrt{\sum_i b_{Si}^2}$ the coupling strength. Since \hat{H}_E does not commute with \hat{H}_{SE} , the effective system-environment interaction $\hat{H}_{SE}^{(E)}$ becomes time-

dependent: the system experiences a coupling to the environment that fluctuates. For a semi-classical treatment we trace over the bath variables, and replace $b_{SE}e^{-i\hat{\mathcal{H}}_E t}\hat{E}_ze^{i\hat{\mathcal{H}}_E t}$ of Eq. (3) by the stochastic function $b_{SE}E_z(t)$ representing a classical random field with a Gaussian distribution with zero average, $\langle E_z(t) \rangle = 0$, and the autocorrelation function $\langle E_z(t)E_z(t+\tau) \rangle = g(\tau)$ [37]. The spectral density of the system-bath interaction is the Fourier transform of $g(\tau)$,

$$S(\omega) = \frac{1}{\sqrt{2\pi}} \int_{-\infty}^{\infty} d\tau g(\tau) e^{-i\omega\tau}. \quad (15)$$

It describes the relative weight of the different frequency components of the SE interaction.

Using this effective field $E_z(t)$, we write the semiclassical SE interaction Hamiltonian as

$$\hat{\mathcal{H}}_{SE}(t) = b_{SE}E_z(t)\hat{S}_z. \quad (16)$$

Clearly, $\hat{\mathcal{H}}_{SE}(t)$ commutes with itself at all times. This allows us to calculate the survival probability

$$s(t) = \frac{\text{Tr} \left\{ e^{-i \int_0^t dt_1 \hat{\mathcal{H}}_{SE}(t_1)} \hat{\rho}_0 e^{i \int_0^t dt_1 \hat{\mathcal{H}}_{SE}(t_1)} \hat{\rho}_0 \right\}}{\text{Tr} \{ \hat{\rho}_0 \hat{\rho}_0 \}} \quad (17)$$

by integrating

$$\int_0^t dt_1 \hat{\mathcal{H}}_{SE}(t_1) = b_{SE} \hat{S}_z \int_0^t dt_1 E_z(t_1) = \phi(t) \hat{S}_z. \quad (18)$$

The survival probability then becomes

$$s(t) = \frac{\text{Tr} \left\{ e^{-i\phi(t)\hat{S}_z} \hat{\rho}_0 e^{i\phi(t)\hat{S}_z} \hat{\rho}_0 \right\}}{\text{Tr} \{ \hat{\rho}_0 \hat{\rho}_0 \}}. \quad (19)$$

If the spin ensemble is initially polarized along the z -direction, $\hat{\rho}_0 = \hat{S}_z$, \hat{S}_z is a constant of motion. However if $\hat{\rho}_0 = \hat{S}_{x,y}$, its survival probability is

$$s_{x,y}(t) = \frac{\text{Tr} \left\{ e^{-i\phi(t)\hat{S}_z} \hat{S}_{x,y} e^{i\phi(t)\hat{S}_z} \hat{S}_{x,y} \right\}}{\text{Tr} \left\{ \hat{S}_{x,y}^2 \right\}} = \cos \phi(t). \quad (20)$$

Taking the average over the random fluctuations

$$\langle s_{x,y}(t) \rangle = \langle \cos \phi(t) \rangle = e^{-\frac{1}{2}\langle \phi^2(t) \rangle}, \quad (21)$$

where we have used $\cos \phi(t) = (e^{i\phi(t)} + e^{-i\phi(t)})/2$ and the property $\langle e^{iX} \rangle = e^{i\langle X \rangle - \langle X^2 \rangle/2}$ for a Gaussian random variable X . For a simple interpretation of the decay, we use the exponential's argument

$$\begin{aligned} \chi(t) &= \frac{1}{2} \langle \phi^2(t) \rangle = \frac{|b_{SE}|^2}{2} \left\langle \int_0^t dt_1 \int_0^t dt_2 E_z(t_1) E_z(t_2) \right\rangle \\ &= \frac{|b_{SE}|^2}{2} \int_{-\infty}^{\infty} dt_1 \int_{-\infty}^{\infty} dt_2 g(t_1 - t_2) f_0(t_1, t) f_0(t_2, t), \end{aligned} \quad (22)$$

where $f_0(t', t) = \Theta(t')\Theta(t - t')$ with the Heaviside function $\Theta(t') = 1 \forall t' > 0$ and zero otherwise. Using Eq. (15), we rewrite this convolution integral as

$$\chi(t) = \frac{\sqrt{2\pi}|b_{SE}|^2}{2} \int_{-\infty}^{\infty} d\omega S(\omega) |F_0(\omega, t)|^2, \quad (23)$$

where $F_0(\omega, t)$ is the Fourier transform of $f_0(t', t)$ [24]

$$\begin{aligned} F_0(\omega, t) &= \frac{1}{\sqrt{2\pi}} \int_{-\infty}^{\infty} dt' f_0(t', t) e^{-i\omega t'} \\ &= \frac{1}{\sqrt{2\pi}} \int_0^t dt' e^{-i\omega t'} = \frac{1}{\sqrt{2\pi}} e^{-i\omega t/2} \frac{\sin(\omega t/2)}{(\omega/2)} \end{aligned} \quad (24)$$

and we have used the fact that the random field E_z is not correlated with the time-domain filter function f . The decay function $\chi(t)$ is thus equal to the product of the spectral density $S(\omega)$ of the system-environment coupling and the filter transfer function $F_0(\omega, t)$.

Here, we have treated the case where no control pulses are applied, which corresponds to the free induction decay. Since both $S(\omega)$ and $|F_0(\omega, t)|^2$ reach their maximum at $\omega = 0$, it is the low frequency environmental noise that has the highest contribution to the decay rate.

B. Analogy between FID and single slit diffraction

Since the decay function $\chi(t)$ arises from the interference between the random fields $E_z(t_1), E_z(t_2)$ at different times, it is helpful to draw an analogy with interference effects in optics. This analogy is best seen with the help of Huygens' principle, which allows us to associate an elementary wave with every point in space; here, we observe interference between elementary waves generated at different points in time and weighted by the filter function $F(\omega, t)$. In the case of free precession (the FID), the time-domain filter function $f_0(t', t)$ is constant over the interval $t' = [0, t]$. This is exactly analogous to the case of diffraction from a slit that extends from 0 to t , and as in the optical case, we obtain a diffraction pattern $\propto |\sin(x)/x|^2$.

According to Eq. (24), the width of the diffraction pattern is $\propto \frac{1}{t}$ and its amplitude $\propto t$. For very short times, i.e., narrow slits, the corresponding diffraction pattern is broader than the width of the spectral density $S(\omega)$ and the integral (23) grows $\sim t^2$. When the time t exceeds the correlation time τ_B of the system-environment interaction, the width of slit broadens and the width of the filter function $F_0(\omega, t)$ becomes narrower than the spectral density pattern $S(\omega)$. In the long time limit $t \gg \tau_B$, the filter function narrows to a delta function at $\omega = 0$ and the decay function becomes $\chi(t) \propto |b_{SE}|^2 S(0)t$, corresponding to an exponential decay. This result is equivalent to the one obtained by Fermi's golden rule and is valid until a power law decay arises [69, 70].

C. Effect of pulses : interference

The effect of DD pulses is a modulation of the time-domain filter function $f(t', t)$ and therefore of the transfer or filter function $F(\omega, t)$. As shown by Eq (23), a slow-down of the decay is achieved by minimizing the overlap between $S(\omega)$ and $|F(\omega, t)|^2$ [24, 27–32]. In the typical case that the environmental spectral density peaks at small frequencies, this implies that $|F(\omega, t)|^2$ should be close to 0 for small frequencies ω .

Let us now study the effect of ideal DD pulses. They generate reversals of $\widehat{\mathcal{H}}_{SE}(t)$, so that the resulting Hamiltonian still commutes with itself at all times. As described in the previous sections, N pulses are applied during the interval τ_c at positions $t_j = \{t_1, t_2, \dots, t_N\}$, with $t_0 = 0$ and $t_{N+1} = \tau_c$. Under this condition, the time-domain filter function $f_N(t', \tau_c)$ in Eq. (22) becomes

$$f_N(t', \tau_c) = \sum_{j=0}^N (-1)^j \Theta(t' - t_j) \Theta(t_{j+1} - t'), \quad (25)$$

where $f_N(t', \tau_c)$ now switches between ± 1 at the position of every pulse [24]. This is depicted in Fig. 7(c) for a cycle of UDD₄. We define τ_{cf} as the period of the filter function $f_N(t', \tau)$. For even DD orders, τ_{cf} is equal to the cycle time τ_c , for odd DD orders, it equals two cycles, i.e., $\tau_{cf} = 2\tau_c$ [Fig. 7(b)].

If the average of the function $f_N(t', \tau_{cf})$ over the period τ_{cf} vanishes, the filter function vanishes at $\omega = 0$

$$|F_N(0, \tau_{cf})| = \frac{1}{\sqrt{2\pi}} \left| \int_{-\infty}^{\infty} dt' f_N(t', \tau_{cf}) \right|^2 = 0. \quad (26)$$

For a general N -pulse sequence, the transfer function $F_N(\omega, t)$ becomes [24]

$$\begin{aligned} F_N(\omega, \tau_{cf}) &= \frac{1}{\sqrt{2\pi}} \int_0^{\tau_{cf}} f_N(t', \tau_{cf}) e^{-i\omega t'} dt' \\ &= \frac{1}{\sqrt{2\pi}} \sum_{j=0}^N (-1)^j \int_{t_j}^{t_{j+1}} e^{-i\omega t'} dt' \\ &= \frac{1}{\sqrt{2\pi}} \frac{1 + (-1)^{N+1} e^{-i\omega \tau_{cf}} + 2 \sum_{j=1}^N (-1)^j e^{-i\omega t_j}}{i\omega}. \end{aligned} \quad (27)$$

Uhrig found a suitable distribution of N pulses over a time τ_{cf} that eliminates the first N derivatives of $\omega F_N(\omega, \tau_{cf})$ [26, 32] and thus it has an optimally flat stop-band at $\omega = 0$.

For a given distribution of pulses, the corresponding time domain filter function is

$$f_N(t', \tau_{cf}) = f_N(t', \infty) \times \Theta(t') \Theta(\tau_{cf} - t'), \quad (28)$$

where $f_N(t', \infty)$ is an infinite extension of the filter function. $f_N(t', \infty)$ can be written as a Fourier series

$$f_N(t', \infty) = \sum_{k=-\infty}^{\infty} A_k \exp(ik\omega_0 t'), \quad (29)$$

where $k\omega_0 = 2\pi k/\tau_{cf}$ are the harmonic frequencies of the period τ_{cf} , and

$$A_k = \frac{\sqrt{2\pi}}{\tau_{cf}} F_N(k\omega_0, \tau_{cf}) \quad (30)$$

the amplitudes. Hence, by convolution, the frequency domain filter has the form,

$$F_N(\omega, \tau_{cf}) = \sum_{k=-\infty}^{\infty} F_N(k\omega_0, \tau_{cf}) e^{-i(\omega - k\omega_0)\tau_{cf}/2} \frac{\sin[(\omega - k\omega_0)\tau_{cf}/2]}{(\omega - k\omega_0)\tau_{cf}/2}. \quad (31)$$

To determine the behavior of $F_N(\omega, \tau_{cf})$ close to $\omega = 0$, it is sufficient to consider the effect of only the first few harmonics on either side of $\omega = 0$. This is shown in Fig. 15 for UDD₄. The red thick line in the lower panel illustrates the stop-band for UDD₄. The blue bars are the Fourier coefficients A_k of the filter function $f_4(t', \infty)$. The contributions of the individual terms in Eq. (31) are represented by the dotted lines in Fig. 15. The sum (interference) of these diffraction effects gives rise to a maximally flat filter shape $|F_N(\omega, \tau_c)|$ close to $\omega = 0$. The top panel of Fig. 15 shows the effect of the addition of diffraction effects of the first two harmonics to the right of $\omega = 0$. The resulting (red thick line) in a region close to $\omega = 0$ is canceled by the corresponding harmonics to the left of $\omega = 0$, as shown in the lower panel.

Physically therefore, the sum in Eq. (27) can be understood as the interference of the diffraction effects due to each inter-pulse delay. In an optical analog, the switching between $f_N(t', \tau_{cf}) = 1 \rightarrow f_N(t', \tau_{cf}) = -1$ corresponds to a phase shift by π , which could be implemented by a series of $\lambda/2$ retardation plates. For short cycle time $\tau_{cf} \ll \tau_B$, the width of this region, where the filter function vanishes, becomes broad compared to the $S(\omega)$ and the integral (23) and thus the decay tend to zero.

D. Effect of cycle iteration: diffraction grating

Let us consider a DD sequence iterated M times for a total period $\tau_M = M\tau_{cf}$. This is illustrated in Fig. 1. The corresponding filter function is then

$$\begin{aligned} F_N(\omega, \tau_M = M\tau_{cf}) &= \frac{1}{\sqrt{2\pi}} \int_0^{\tau_{cf}} f_N(t', \tau_{cf}) e^{-i\omega t'} dt' \times \\ &\quad \times \left[1 + e^{-i\omega \tau_c} + e^{-i2\omega \tau_{cf}} + \dots + e^{-i(M-1)\omega \tau_{cf}} \right] \\ &= \frac{\sin\left(\frac{M\omega \tau_{cf}}{2}\right)}{\sin\left(\frac{\omega \tau_{cf}}{2}\right)} e^{-\frac{i\omega(M-1)\tau_{cf}}{2}} \frac{1}{\sqrt{2\pi}} \int_0^{\tau_{cf}} f_N(t', \tau_{cf}) e^{-i\omega t'} dt' \\ &= \frac{\sin\left(\frac{M\omega \tau_{cf}}{2}\right)}{\sin\left(\frac{\omega \tau_{cf}}{2}\right)} e^{-\frac{i\omega(M-1)\tau_{cf}}{2}} F_N(\omega, \tau_{cf}). \end{aligned} \quad (32)$$

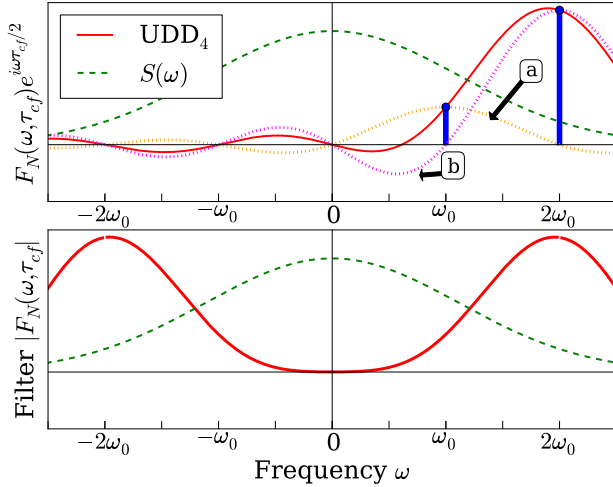


Figure 15: (Color online) Decomposition of the filter function $F_N(\omega, \tau_{cf})$ for the UDD_4 sequence. Blue bars mark the contributions of the harmonics of $\omega_0 = 2\pi/\tau_{cf}$. Orange and magenta dotted lines labeled a and b are sinc functions centered at ω_0 and $2\omega_0$. The top panel considers the effect only of the first two harmonics ($k = 1, 2$). They interfere to give the resulting red thick line. The bottom panel shows how a region near to $\omega = 0$ is completely canceled when we also consider the contribution of the two harmonics with $k = -1, -2$. The green dashed line is a typical Gaussian spectral density function of the spin-bath.

This is analogous to the intensity pattern obtained due to diffraction from an M -line grating. The maxima of the filter function $|F_N(\omega, \tau_M)|$ again occur at the harmonic frequencies $\omega = 2\pi k/\tau_{cf}$, where k is an integer. These are the peaks of the blue bars in Fig. 15 and Fig. 16(a) for UDD_4 , and the red bars in Fig. 16(d) for CPMG. Their amplitudes are given by the filter function $F_N(\omega, \tau_{cf})$ of a single cycle which is shown by blue and red dotted lines in Fig. 16(a) and (b). For different even UDD orders the single cycle filter functions $F_N(\omega, \tau_{cf})$ are shown in Fig. 16(b) and the respective harmonic positions are represented by the empty circles. Between two of the principal maxima (harmonics) are $(M - 2)$ secondary maxima, which are determined by the grating transfer function $\sin(M\omega\tau_{cf}/2)/\sin(\omega\tau_{cf}/2)$. As shown in Fig. 16(a) and (d) on the solid lines and in panel (c), their amplitudes with respect to the principal maximum falls off $\propto M^{-1}$. For example, with only 6 cycles, the intensity of the first secondary maximum is less than 5% of the maximum. Note that in Fig. 16 $|F_N(\omega, \tau_{cf})|$ is plotted; the contribution of the secondary maxima is drastically reduced after taking the square.

Hence for even a few cycles, the filter function $|F_N(\omega, \tau_M)|$ becomes an almost discrete spectrum that is given by the discrete Fourier transform of $f_N(t', \tau_{cf})$. This is just the function $f_N(t', \infty)$. Fig. 16 shows the

comparison of the filter functions $F_N(\omega, \tau_M)$ for UDD_4 [panel (a): blue solid line] with $M = 12$ and CPMG [panel (d): red solid line] with $M = 24$. The latter choice allows us to have the same evolution time for a fair comparison. The ω_0 in the frequency axis is defined in terms of the cycle time for CPMG,

$$\omega_0 = 2\pi/(\tau_{cf}^{\text{CPMG}}) = 2 \times 2\pi/(\tau_{cf}^{\text{UDD}_4}). \quad (33)$$

Figure 16(c) shows $F_N(\omega, \tau_M)$ for different UDD orders iterated to match the same total evolution time. In Fig. 15 and Fig. 16(a) and (d), the spectrum corresponding to $F_N(\omega, \infty)$ contains only the blue bars (for UDD_4) or the red bars (for CPMG). Equivalently on Fig. 16(b), it is given by the empty circles. The decay function $\chi(t)$ is thus a weighted sampling of the spectral density function $S(\omega)$, where the weighting factor is the magnitude of the respective Fourier components. Thus,

$$\chi(t = \tau_M) \propto \tau_M b_{SE}^2 \sum_k A_k^2 S(k\omega_0). \quad (34)$$

Here, we have assumed $t = \tau_M \gg \tau_B$ so that $F(\omega, t)$ is well represented by a series of δ -functions centered at $k\omega_0$, given by $F_N(\omega, \infty)$, while the contributions from the secondary maxima can be neglected.

This decay function (34) is equivalent to the one derived by standard time dependent perturbation theory for a spin interacting with a continuum of states. The result is similar to an expression derived by Fermi's golden rule but the spectral density $S(\omega)$ is evaluated on the frequency components of the time-dependent perturbation

$$\hat{\mathcal{H}}_{SE}(t) = b_{SE} \left[\sum_k A_k \cos(k\omega_0 t) \right] E_z(t) \hat{S}_z. \quad (35)$$

It follows that for large M , the main contribution to the decay rate is determined by the spectral density $S(\omega)$ at the harmonic frequencies $k\omega_0$. The lowest frequency component present in a DD sequence is the inverse of the period τ_{cf} of the time domain filter. The CPMG sequence has the shortest period if the average distance between pulses τ is fixed: $\tau_{cf}^{\text{CPMG}} = 2\tau$ and $\omega_0^{\text{CPMG}} = \pi/(\tau)$. For an N pulse UDD cycle the period of the filter function in the time-domain is $\tau_{cf}^{\text{UDD}_N} = N\tau$ ($\tau_{cf}^{\text{UDD}_N} = 2N\tau$) for N even (odd). Thus the first non-vanishing component in its Fourier expansion is at $\omega_0^{\text{UDD}_N} = 2\pi/(N\tau)$ ($\omega_0^{\text{UDD}_N} = \pi/(N\tau)$) [Fig. 16]. In the system studied here, this has resulted in the CPMG generating the slowest decay.

E. Simulations

For the longitudinal initial condition flip-angle errors are well compensated as was shown in Ref. [38]. As a consequence, the effect of static pulse imperfections and finite pulse lengths in the experiments does not cause a qualitative difference to the simulations with ideal pulses.

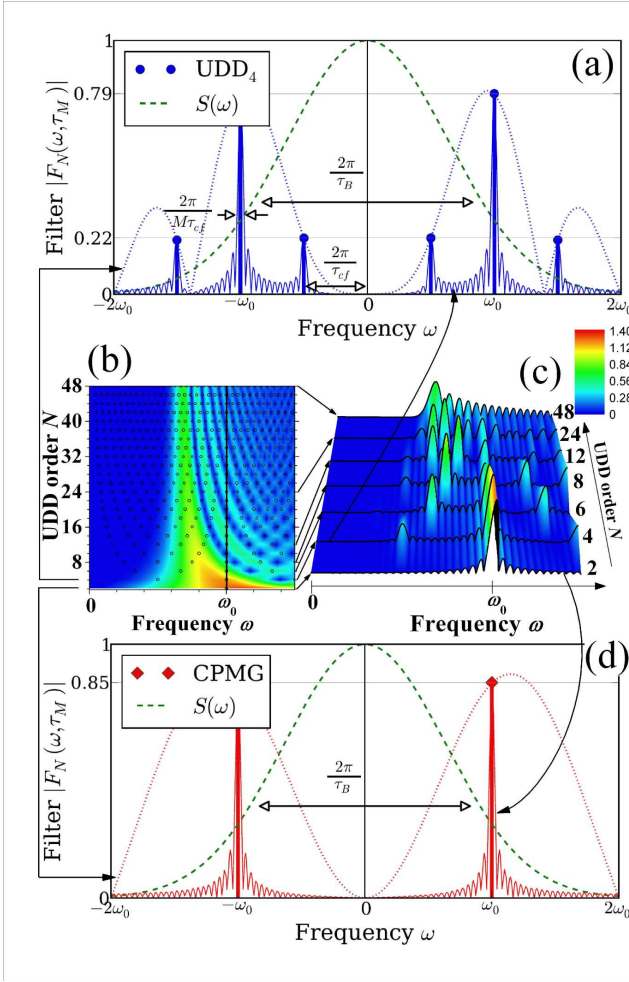


Figure 16: (Color online) Comparison of filter functions $|F_N(\omega, \tau_M)|$ for different UDD orders: (a) UDD_4 with $M = 1$ (dotted line) and $M = 12$ (solid line), even UDD orders N with $M = 1$ (b) and $M = 48/N$ (c), and (d) $\text{CPMG} = \text{UDD}_2$ with $M = 1$ (dotted line) and $M = 24$ (solid line). ω_0 is defined in terms of the cycle time of the CPMG sequence, $\omega_0 = 2\pi/\tau_{cf}^{\text{CPMG}}$. Blue circles (a), red rhombuses (d) and empty circles in (b) are the coefficients of the Fourier expansion of $f_N(t', \infty)$. They are modulated by the shape of the filter function $|F_N(\omega, \tau_{cf})|$, shown in panel (b) and represented by blue and red dotted lines in panels (a) and (d), where $\tau_{cf}^{\text{CPMG}} = 2\tau$ and $\tau_{cf}^{\text{UDD}_N} = N\tau$.

We therefore assume ideal DD pulses and Eqs. (23) and (32) allow us to simulate the resulting signal decays. However, for the transverse initial condition, the pulse errors are not compensated [38]. Thus, here we only describe how the simulations for the longitudinal case were carried out.

First, the spectral density $S(\omega)$ used in Eq. (23) is estimated using the FIDs of Fig. 5, as described in section IV.A of Ref. [38]. We model a finite system to simulate the respective correlation functions that produce the experimentally measured FIDs for both nuclei (see [38] for details). The correlation time of the bath is defined as

the time when the correlation function falls to $1/e$ of the initial value; this was found to be around $\tau_B = 110\mu\text{s}$.

Now, including the DD pulses, $\chi(t)$ is calculated after every cycle period τ_c following Eq. (23) and (32). The decay rate is determined by linearly fitting the values of $\chi(t)$ obtained for different times. This procedure is exact for the case when the decay is purely exponential – for example, when the time t far exceeds the correlation time of the bath as described above. These simulations (lines) show reasonable agreement with the real experimental results in Figs. 8, 11 and 12.

F. Discussion

Visualizing dynamical decoupling as a filter [24, 25] for different frequency components of the environmental noise provides a useful means for predicting relative DD performance. Some recent discussions by Biercuk and Uys [25] about the filter properties of different DD sequences concerning their Fourier components has appeared in parallel with our work. However, their work and ours contribute from different approaches: we compare the performance of different DD orders under the condition that the number of pulses applied during a time interval remains constant, while Biercuk and Uys fix the cycle time for every DD order.

Although the UDD sequence that was derived from Eq. (27) has a flatter band-stop region close to $\omega = 0$, it achieves this by the interference of a larger number of harmonic frequencies lower than the first harmonic of an equidistant sequence (CPMG) with the same average spacing τ between the pulses. This is illustrated in Fig. 16. The first non-zero Fourier component of the CPMG occurs at $\omega_0^{\text{CPMG}} = \pi/\tau$, while for an N -pulse UDD sequence it occurs at $\omega_0^{\text{UDD}_{\text{even}}} = \omega_0^{\text{CPMG}}/N$ [$\omega_0^{\text{UDD}_{\text{odd}}} = \omega_0^{\text{CPMG}}/(2N)$]. Therefore, as one increases the UDD order, additional components appear in the corresponding frequency-domain filter function at frequencies below ω_0^{CPMG} .

We may thus compare the effect of two contributions to the decay rate: The spectral density close to the lowest frequency component ω_0 and the integral over the frequency band close to $\omega = 0$. UDD is designed to outperform CPMG in this low-frequency band and thus superior if this is the dominant contribution. However, in the system that we are considering here, the spectral density of the environmental noise is still sufficiently large at ω_0^{UDD} that this term dominates and leads to UDD performing worse than CPMG.

Previous works [42, 43] used perturbation treatment of the SE interaction to predict the time evolution of the system under UDD at short times with high precision. However, the regimes where the decay is reduced by increasing the UDD order lead in general to differences between their decays of order lower than 10^{-4} which are too small to be determined experimentally. The extrapolation of those decays to longer times, by means of

iterating the DD sequences, that may result in a magnification of the UDD performance relative to CPMG is not valid within the perturbative treatment. Our analysis, in contrast, is valid for times $t \gg \tau_B$, where decay becomes appreciable ($>1\%$) and thus experimentally accessible. The filter function $F_N(\omega, M\tau_{cf})$ now becomes discrete when M is large and changes drastically the decay compared to the extrapolation from a perturbative treatment of the SE interaction. From a different approach, this situation was also observed by Khodjasteh *et al.* [45] for a bosonic bath: they noticed that an extrapolation could not be done and they obtained bounds for the UDD performance as a function of its order. Our results suggest that to achieve a parameter range where UDD would outperform CPMG would correspond to an almost static bath, i.e., the system-environment interaction $|b_{SE}|^2$ should be much stronger than the relevant intra-bath interactions.

Our model may also explain the observation in [33] where the odd UDD orders were found to perform substantially worse than even orders in a qubit system consisting of $^9\text{Be}^+$ ions confined in a Penning trap, and where the $S(\omega) \sim 1/\omega^4$. This even-odd asymmetry was unexplained in their paper [33].

VII. CONCLUSIONS

We have presented experimental and theoretical results evaluating the relative performance of DD sequences with non-equidistant pulses in a purely-dephasing spin-bath. We find that over a large range of cycle times, number of pulses per cycle and bath-correlation time, the equidistant sequence (CPMG) provides a measurably superior performance over non-equidistant sequences like UDD. If the rotation axis of the DD pulses is oriented in the direction of the initial state, we find that the experimental results match very well with simulations using the filter model for perfect pulses [24]. In this case, the effects due to the finite pulse-length, and flip-angle errors do not qualitatively affect the results.

We interpret our results through a semi-classical model by drawing an analogy of dynamical decoupling with interference effects in optics and filter theory. The CPMG sequence has the shortest cycle and its filter has the

widest stop-band. By suitable interferences, the UDD filter has the flattest stop-band close to $\omega = 0$. In our system, the position of the lowest frequency component is more important than the very flat behavior of UDD, and thus the performance of CPMG is better than that of non-equidistant DD sequences. We show that this comes from the fact that the decay rate changes drastically from short to long times compared with the bath-correlation time. While for short evolution times, the flattest stop-band close to $\omega = 0$ may play an important role in reducing the decay rate, the fidelity reduction is $< 10^{-4}$ and thus too small to be observed experimentally. The extrapolation of those decays to longer times that may result in a magnification of the UDD performance relative to CPMG is not valid. In contrast, we showed that for long times, where decay becomes appreciable, the filter function becomes discrete, making CPMG superior because its frequency components have the widest spacing. Conversely, we expect that UDD should perform better in systems where the cycle time remains significantly shorter than the bath correlation time.

Our results and the optical analogy we considered reaffirm that it would be advantageous to tailor the DD sequence to the spectral density function of the noise in the particular system of interest. This is the basis behind the Locally Optimized DD (LODD) sequences [25, 28, 29, 31, 36] or similar [27, 30]. In particular LODD can be implemented using measurement feedback in order to find the optimal DD sequence [28]. However, more work needs to be done in methods for experimentally determining the exact noise features in the QIP system of choice, so that techniques like LODD could be used to determine optimal sequences for such environments.

Acknowledgments

This work is supported by the DFG through Su 192/24-1. GAA thanks the Alexander von Humboldt Foundation for a Research Scientist Fellowship. We thank Götz Uhrig, Stefano Pasini and Daniel Lidar for helpful discussions, and Marko Lovric and Ingo Niemeyer for technical support. We thank Michael Biercuk for some useful comments about our manuscript.

-
- [1] M. A. Nielsen and I. L. Chuang, *Quantum Computation and Quantum Information* (Cambridge University Press, Cambridge, 2000).
 - [2] J. Preskill, P. Roy. Soc. Lond. A Mat. **454**, 385 (1998).
 - [3] W. H. Zurek, Rev. Mod. Phys. **75**, 715 (2003).
 - [4] G. DeChiara, D. Rossini, S. Montangero, and R. Fazio, Phys. Rev. A **72**, 012323 (2005).
 - [5] C. K. Burrell and T. J. Osborne, Phys. Rev. Lett. **99**, 167201 (2007).
 - [6] J. Allcock and N. Linden, Phys. Rev. Lett. **102**, 110501 (2009).
 - [7] G. A. Álvarez and D. Suter, Phys. Rev. Lett. **104**, 230403 (2010).
 - [8] P. W. Shor, in *Proceedings of the 35th Annual Symposium on the Foundations of Computer Science*, edited by S. Goldwasser (IEEE Computer Society Press, Los Alamitos, CA, 1994), p. 124.
 - [9] L. Viola, E. Knill, and S. Lloyd, Phys. Rev. Lett. **82**, 2417 (1999).
 - [10] W. Yang, Z. Wang, and R. Liu, arXiv:1007.0623 (2010).

- [11] J. M. Taylor, P. Cappellaro, L. Childress, L. Jiang, D. Budker, P. R. Hemmer, A. Yacoby, R. Walsworth, and M. D. Lukin, *Nat. Phys.* **4**, 810 (2008).
- [12] L. T. Hall, C. D. Hill, J. H. Cole, and L. C. L. Hollenberg, *Phys. Rev. B* **82**, 045208 (2010).
- [13] G. de Lange, D. RistÅš, V. V. Dobrovitski, and R. Hanson, arXiv:1008.4395 (2010).
- [14] S. Boixo and R. D. Somma, *Phys. Rev. A* **77**, 052320 (2008).
- [15] E. L. Hahn, *Phys. Rev.* **80**, 580 (1950).
- [16] H. Y. Carr and E. M. Purcell, *Phys. Rev.* **94**, 630 (1954).
- [17] S. Meiboom and D. Gill, *Rev. Sci. Instrum.* **29**, 688 (1958).
- [18] L. Viola, S. Lloyd, and E. Knill, *Phys. Rev. Lett.* **83**, 4888 (1999).
- [19] L. Viola and E. Knill, *Phys. Rev. Lett.* **90**, 037901 (2003).
- [20] K. Khodjasteh and L. Viola, *Phys. Rev. Lett.* **102**, 080501 (2009).
- [21] K. Khodjasteh, D. A. Lidar, and L. Viola, *Phys. Rev. Lett.* **104**, 090501 (2010).
- [22] J. R. West, D. A. Lidar, B. H. Fong, M. F. Gyure, X. Peng, and D. Suter, arXiv:0911.2398 (2009).
- [23] J. R. West, B. H. Fong, and D. A. Lidar, *Phys. Rev. Lett.* **104**, 130501 (2010).
- [24] L. Cywinski, R. M. Lutchyn, C. P. Nave, and S. Das-Sarma, *Phys. Rev. B* **77**, 174509 (2008).
- [25] M. J. Biercuk and H. Uys, arXiv:1012.4262 (2010).
- [26] G. S. Uhrig, *Phys. Rev. Lett.* **98**, 100504 (2007).
- [27] G. Gordon, G. Kurizki, and D. A. Lidar, *Phys. Rev. Lett.* **101**, 010403 (2008).
- [28] M. J. Biercuk, H. Uys, A. P. VanDevender, N. Shiga, W. M. Itano, and J. J. Bollinger, *Nature* **458**, 996 (2009).
- [29] H. Uys, M. J. Biercuk, and J. J. Bollinger, *Phys. Rev. Lett.* **103**, 040501 (2009).
- [30] J. Clausen, G. Bensky, and G. Kurizki, *Phys. Rev. Lett.* **104**, 040401 (2010).
- [31] Y. Pan, Z.-R. Xi, and W. Cui, *Phys. Rev. A* **81**, 022309 (2010).
- [32] G. S. Uhrig, *New J. Phys.* **10**, 083024 (2008).
- [33] M. J. Biercuk, H. Uys, A. P. VanDevender, N. Shiga, W. M. Itano, and J. J. Bollinger, *Phys. Rev. A* **79**, 062324 (2009).
- [34] E. R. Jenista, A. M. Stokes, R. T. Branca, and W. S. Warren, *J. Chem. Phys.* **131**, 204510 (2009).
- [35] J. Du, X. Rong, N. Zhao, Y. Wang, J. Yang, and R. B. Liu, *Nature* **461**, 1265 (2009).
- [36] S. Pasini and G. S. Uhrig, *Phys. Rev. A* **81**, 012309 (2010).
- [37] A. Abragam, *Principles of Nuclear Magnetism* (Oxford University Press, London, 1961).
- [38] G. A. Álvarez, A. Ajoy, X. Peng, and D. Suter, *Phys. Rev. A* **82**, 042306 (2010).
- [39] G. de Lange, Z. H. Wang, D. Riste, V. V. Dobrovitski, and R. Hanson, *Science* **330**, 60 (2010).
- [40] C. Barthel, J. Medford, C. M. Marcus, M. P. Hanson, and A. C. Gossard, arXiv:1007.4255 (2010).
- [41] C. A. Ryan, J. S. Hodges, and D. G. Cory, *Phys. Rev. Lett.* **105**, 200402 (2010).
- [42] G. S. Uhrig and D. A. Lidar, *Phys. Rev. A* **82**, 012301 (2010).
- [43] T. E. Hodgson, L. Viola, and I. D'Amico, *Phys. Rev. A* **81**, 062321 (2010).
- [44] K. Chen and R.-B. Liu, arXiv:1009.0984 (2010).
- [45] K. Khodjasteh, T. Erdélyi, and L. Viola, arXiv:1009.1810 (2010).
- [46] G. S. Uhrig and S. Pasini, *New J. Phys.* **12**, 045001 (2010).
- [47] B. Naydenov, F. Dolde, L. T. Hall, C. Shin, H. Fedder, L. C. L. Hollenberg, F. Jelezko, and J. Wrachtrup, arXiv:1008.1953 (2010).
- [48] H. Bluhm, S. Foletti, I. Neder, M. Rudner, D. Mahalu, V. Umansky, and A. Yacoby, arXiv:1005.2995 (2010).
- [49] R. Hanson, L. P. Kouwenhoven, J. R. Petta, S. Tarucha, and L. M. K. Vandersypen, *Rev. Mod. Phys.* **79**, 1217 (2007).
- [50] B. E. Kane, *Nature* **393**, 133 (1998).
- [51] J. J. L. Morton, A. M. Tyryshkin, R. M. Brown, S. Shankar, B. W. Lovett, A. Ardavan, T. Schenkel, E. E. Haller, J. W. Ager, and S. A. Lyon, *Nature* **455**, 1085 (2008).
- [52] F. Dyson, *Phys. Rev.* **75**, 486 (1949).
- [53] F. Dyson, *Phys. Rev.* **75**, 1736 (1949).
- [54] U. Haeberlen, *High Resolution NMR in Solids: Selective Averaging* (Academic Press, New York, 1976).
- [55] W. Magnus, *Commun. Pure Appl. Math.* **7**, 649 (1954).
- [56] K. Khodjasteh and D. A. Lidar, *Phys. Rev. Lett.* **95**, 180501 (2005).
- [57] U. Haeberlen and J. S. Waugh, *Phys. Rev.* **185**, 420 (1969).
- [58] W. Rhim, D. P. Burum, and D. D. Elleman, *Phys. Rev. Lett.* **37**, 1764 (1976).
- [59] M. B. Franzoni and P. R. Levstein, *Phys. Rev. B* **72**, 235410 (2005).
- [60] D. Li, A. E. Dementyev, Y. Dong, R. G. Ramos, and S. E. Barrett, *Phys. Rev. Lett.* **98**, 190401 (2007).
- [61] M. B. Franzoni, P. R. Levstein, J. Raya, and J. Hirschinger, *Phys. Rev. B* **78**, 115407 (2008).
- [62] D. Li, Y. Dong, R. G. Ramos, J. D. Murray, K. MacLean, A. E. Dementyev, and S. E. Barrett, *Phys. Rev. B* **77**, 214306 (2008).
- [63] Y. Dong, R. G. Ramos, D. Li, and S. E. Barrett, *Phys. Rev. Lett.* **100**, 247601 (2008).
- [64] W. Yang and R. Liu, *Phys. Rev. Lett.* **101**, 180403 (2008).
- [65] A. Pines, M. G. Gibby, and J. S. Waugh, *J. Chem. Phys.* **56**, 1776 (1972).
- [66] K. Khodjasteh and D. A. Lidar, *Phys. Rev. A* **75**, 062310 (2007).
- [67] D. Burum, M. Linder, and R. Ernst, *Journal of Magnetic Resonance* (1969) **44**, 173 (1981).
- [68] M. Ernst, A. Verhoeven, and B. H. Meier, *J. Magn. Reson.* **130**, 176 (1998).
- [69] E. R. Fiori and H. M. Pastawski, *Chem. Phys. Lett.* **420**, 35 (2006).
- [70] G. A. Álvarez, E. P. Danieli, P. R. Levstein, and H. M. Pastawski, *Phys. Rev. A* **82**, 012310 (2010).